Molecular fractionation in melt-crystallized polyethylene: 4. Fracture*

U. W. Gedde and J.-F. Jansson
Department of Polymer Technology, The Royal Institute of Technology, S-100 44 Stockholm, Sweden
(Received 28 October 1983; revised 5 November 1984)

The macroscopically brittle fracture of five high-density polyethylenes subjected to different constant uniaxial tensile loads was studied by s.e.m. fractography on both untreated and solvent-etched samples. The low molecular weight systems showed three types of fracture propagation: interspherulitic propagation with and without reorientation and trans-spherulitic interlamellar propagation. There is evidence that the development of fracture is associated with a strength distribution in the structure caused by molecular weight segregation occurring during solidification of the samples.

(Keywords: high-density polyethylene; fracture; molecular fractionation; morphology; model calculation; fold surface; thermal treatment)

INTRODUCTION

The subject of this paper, the fifth in a series[1-4] dealing with molecular fractionation in melt-crystallized polyethylene (PE), is the relationship between the development of fracture in isotropic melt-crystallized PE and the morphology of the material. Particular attention is paid to the path of fracture in relation to morphological structural units such as spherulites and crystal lamellae. The purpose of the work has been to substantiate the different fracture modes in more fundamental terms, i.e. to identify weak parts of the structure and to explain their origin on the basis of crystallization kinetics. Data are also presented showing the influence of thermal treatment on the fracture properties of the materials. Polarized light microscopy (p.m.) and electron microscopy (e.m.) have revealed information concerning the fracture of isotropic melt-crystallized PE:

- In bulk specimens, at liquid nitrogen temperatures, fracture frequently propagates along a path containing crystal–amorphous boundaries[5].
- When 3–30 μm films (Marlex 50) were drawn at 300 K some preference was shown for yielding and for the formation of holes at spherulite boundaries[6]. Annealing made the films brittle and they ruptured along the spherulite boundaries[6]. The authors pointed out that the thickness of the films was reduced at the spherulite boundaries and they could not exclude the possibility that the fracture path was controlled by this thickness variation.
- Linear PE samples with very coarse spherulites, formed at high crystallization temperatures, undergo brittle fracture at very low stresses and strains and the path of fracture is irregular regardless of spherulite structure and direction of fibrils[7]. Samples with spherulites of less coarse texture, grown at lower temperatures, undergo fracture localized to the spherulite boundaries[7]. More finely textured samples of the same PE underwent yield[7].
- Fotheringham and Parker[8] have presented data indicating a geometric dependence of fracture. Within a sector of the spherulite $\pm 45°$ to the tensile axis, circumferential cracks are formed. Elsewhere the cracks formed have a perpendicular orientation.

EXPERIMENTAL

Dumb-bell shaped specimens (length of narrow section = 60 mm, radius of narrowing section = 40 mm) were machined and polished (to remove surface irregularities and any oxidized surface layer) from 3 mm sheets produced by compression moulding. The sheets produced from the PEs, whose characterization is given in *Table 1*, and were subjected to two different thermal treatments.

- Rapid cooling (50–80 K min^{-1}) from 450 K to 300 K. The samples produced in this manner are here referred to as RC samples.
- Crystallization from the melt at 398.2 K for 24 h followed by a rapid cooling (50–80 K min^{-1}) to 300 K (IC samples).

The time to fracture was recorded under different constant uniaxial tensile loads at different constant temperatures ranging from 303 K to 353 K. Two of the polyethylenes, 2912 and 2215, were tested in water to obtain brittle fracture within a reasonable time, whereas the

Table 1 Polyethylenes investigated

Material code	$\bar{M}_n \times 10^{-3}$ [a]	$\bar{M}_w \times 10^{-3}$ [a]	MI_2 [b]	Density (kg m^{-3}) [c]
7022	7.4	51	22	963
7018	9.5	80	18	963
7006	8.4	90	7	960
2912	21.6	199	0.3	957
2215	22.0	286	0.05	953

[a] By gel permeation chromatography.
[b] Melt flow index according to ISO/R 292.
[c] On the material as obtained from the manufacturer according to ASTM D 1505-68.

* A part of this paper was presented at the 'Nordic Polymer Symposium', Stockholm, Sweden, January 1983.

0032-3861/85/101469-08$03.00

samples of the other materials were fractured in air.

The fracture surfaces were examined in the scanning electron microscope (s.e.m.), an ISI Super Mini SEM, with no treatment other than gold-sputtering. The thickness of the gold layer is 20 nm.

Some samples containing the fracture surface were treated with hot *p*-xylene in order selectively to dissolve the so-called segregated component. More detailed information concerning the solvent treatments is given in previous reports[3,9]. The main purpose of the solvent treatment was to make the lamellar structure and other morphological structures observable with reference to the fracture surface. The solvent-treated samples were finally subjected to gold-sputtering and s.e.m. examination.

RESULTS AND DISCUSSION

The development of fracture in low molecular weight PE

When the molecular weight of a PE sample is sufficiently low, fracture is macroscopically brittle regardless of stress[10], but s.e.m. fractography provides evidence for the formation of small fibrils accompanying fracture[4]. There are three phases in the development of fracture in a system subjected to a constant uniaxial tensile load[11]:

- Firstly, there is a period with no observable crack growth.
- Secondly, there is a period of slow crack growth during which the stress intensity factor is less than K_{IC}. A circular or semicircular fracture surface is formed during this period.
- Finally, there is a period of rapid crack growth during which the stress intensity factor is larger than K_{IC}.

It was reported in a previous paper[4] that interspherulitic propagation is dominant both in the slow crackgrowth region and in the rapid crackgrowth region for samples of 7006-IC. The same behaviour is observed in the other polyethylenes showing macroscopic brittle fracture, 7022-IC, 7022-RC, 7006-RC, 7018-IC and 7018-RC. This type of fracture is shown in *Figures 1a* and *b*. In no case was there any indication of the presence of foreign particles in the centre of the slow crackgrowth region, as has often been observed in fracture surfaces of polymers.

In addition to interspherulitic propagation there is evidence for a trans-spherulitic interlamellar propagation (*Figures 1c–g*). The features of these micrographs are as follows:

- There is a correspondence in both size and shape between the circular regions observed in the fracture surfaces and the spherulites observed by polarized microscopy.
- The circular regions appear to be the result of interlamellar fracture. The sharp edges generally have a radial orientation and they are frequently very pronounced in the centre of the circular regions as illustrated in *Figure 1c*.

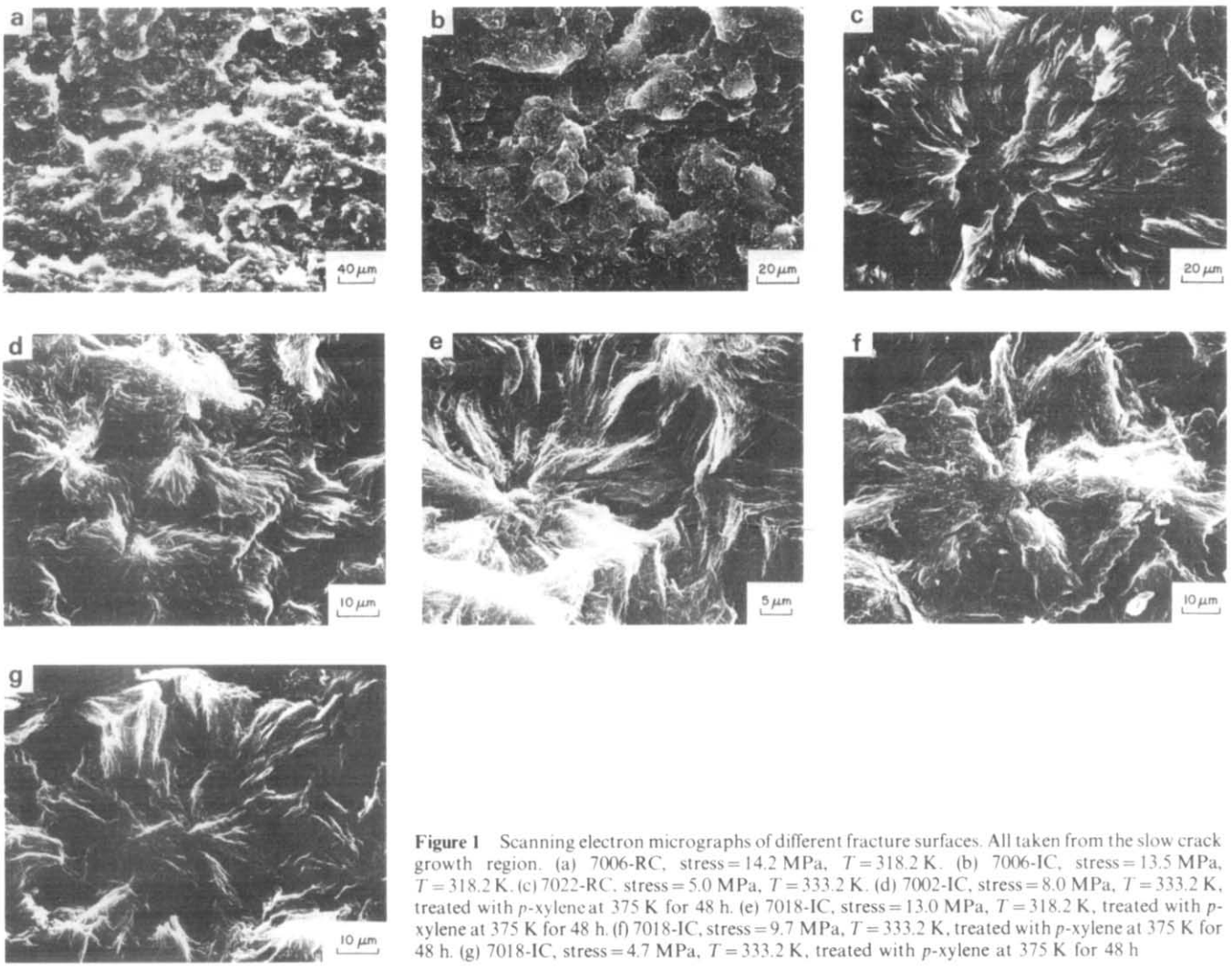

Figure 1 Scanning electron micrographs of different fracture surfaces. All taken from the slow crack growth region. (a) 7006-RC, stress = 14.2 MPa, T = 318.2 K. (b) 7006-IC, stress = 13.5 MPa, T = 318.2 K. (c) 7022-RC, stress = 5.0 MPa, T = 333.2 K. (d) 7002-IC, stress = 8.0 MPa, T = 333.2 K, treated with *p*-xylene at 375 K for 48 h. (e) 7018-IC, stress = 13.0 MPa, T = 318.2 K, treated with *p*-xylene at 375 K for 48 h. (f) 7018-IC, stress = 9.7 MPa, T = 333.2 K, treated with *p*-xylene at 375 K for 48 h. (g) 7018-IC, stress = 4.7 MPa, T = 333.2 K, treated with *p*-xylene at 375 K for 48 h

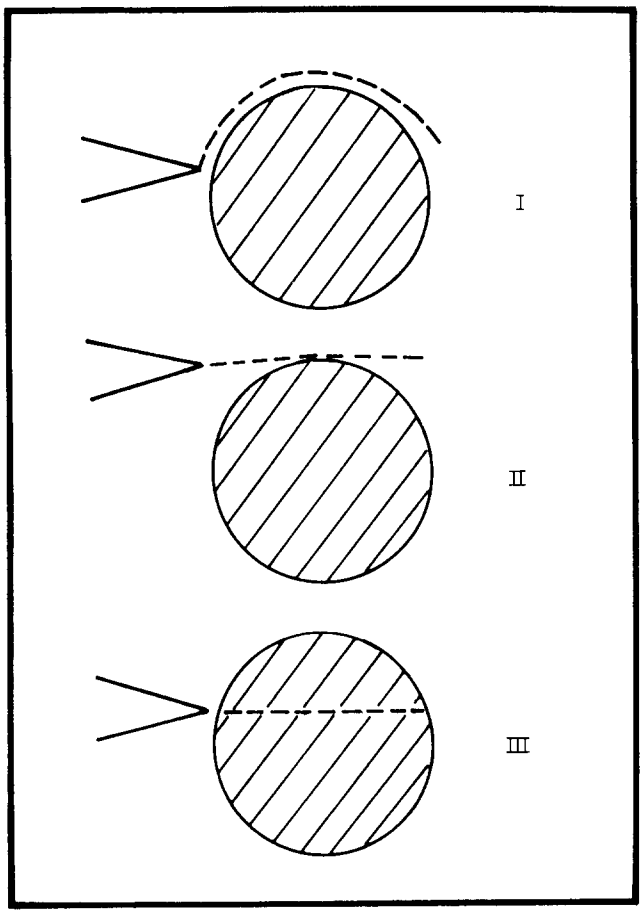

Figure 2 Generalized fracture propagation modes: (I) Interspherulitic propagation with reorientation. (II) Interspherulitic propagation without reorientation. (III) Trans-spherulitic interlamellar propagation

- The micrographs of the solvent-etched fracture surfaces (*Figures 1d–g*) show that the stacks of parallel crystal lamellae are arranged parallel to the fracture surface confirming the interlamellar character of the fracture propagation. The spherulite origin of the circular regions on the fracture surface is demonstrated by the radial orientation of the lamellae.

There are thus three types of fracture propagation, as shown in *Figure 2*: interspherulitic propagation with reorientation (change of direction) (mode I), interspherulitic propagation without reorientation (mode II) and trans-spherulitic interlamellar propagation (mode III).

In the simple case of a uniaxial tensile stress, the fracture should propagate in a direction perpendicular to the stress. Any deviation from this behaviour indicates a non-uniform distribution of strength in the system. One type of distribution arises from the existence of amorphous and crystalline regions. The greater strength of the crystalline regions has been confirmed experimentally[12–14]. In addition, the variation in strength between different amorphous regions should be considered. In principle, amorphous regions with a high concentration of interlamellar tie chains should be stronger than amorphous regions with a low concentration of tie chains, for two reasons: (i) A tie chain can store considerably more elastic energy than other types of amorphous chains (chain folds and cilia) and (ii) a tie chain can transfer stresses between different lamellae more efficiently than both chain folds and cilia. Hence, a considerable amount of elastic energy can be dissipated into heat due to structural rearrangements (yielding) by this efficient transfer of stress. It is therefore important to know how the tie chain concentration varies with other measurable molecular and morphological properties. The concentration of interlamellar tie chains is estimated as a function of molecular weight, crystallinity, lamellar thickness and chain tilt by the following model calculation:

The polymer is assumed to consist only of linear molecules and is considered to be arranged as shown in *Figure 3*, i.e. to be a two component system composed of lamellar crystals (thickness $=L_c$) with a mass fraction (crystallinity) of W_c and amorphous regions (thickness $=L_a$) localized between the crystal lamellae. The molecules in the crystals are assumed to be tilted at an angle θ with respect to the normal to the fold surface.

The amorphous regions contain three types of molecule: interlamellar tie chains connecting different crystal lamellae, chain folds or loops, and molecules containing chain ends (cilia) which are excluded from the crystals[15].

According to the model, the concentration of chain ends in the amorphous phase, C_{ca}, is related to the 'local' molecular weight (M) and to the 'local' crystallinity as follows:

$$C_{ca} = 2\rho_a/(M(1-W_c)) \quad (1)$$

where ρ_a is the density of the amorphous component.

The concentration of tie chain entries (N_t) and loop entries (N_l) in the fold surface of a system arranged as shown in *Figure 3* is calculated from a simple balance equation. The number of molecular entries to the amorphous interlayer is equal to the sum of half the number of chain ends (as given by equation (1)), the number of tie chain entries and the number of fold entries:

$$N_t + N_l = N_{eo}\cos\theta - L_a\rho_a/(M(1-W_c)) \quad (2)$$

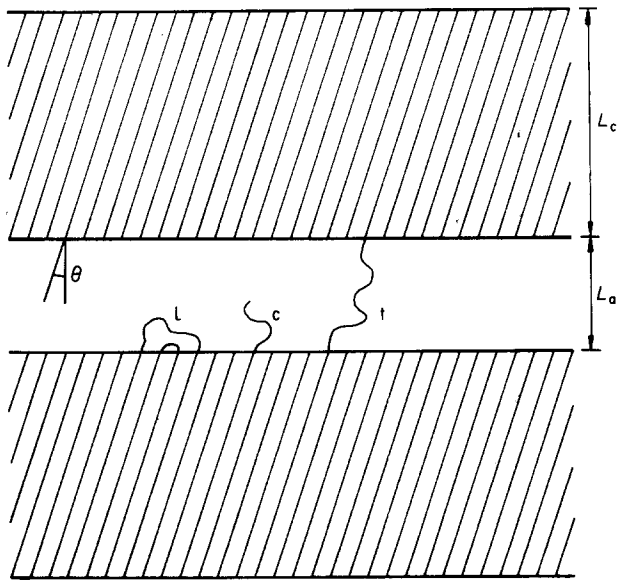

Figure 3 Model of semi-crystalline polymers featuring a part of a stack of lamellar crystals and alternating amorphous interlayers, including definitions of crystal thickness (L_c), thickness of amorphous interlayer (L_a) and chain tilt angle (θ)

where N_{eo} is the number of molecular entries with tilt angle $\theta = 0°$ to the amorphous interlayer per unit area of fold surface. The thickness, L_a, of the amorphous interlayer can be eliminated from equation (2) by considering the two-component character of the studied system (equation (3)), viz.:

$$L_a = L_c\rho_c(1 - W_c)/(W_c\rho_a) \quad (3)$$

$$N_t + N_l = N_{eo}\cos\theta - L_c\rho_c/(W_cM) \quad (4)$$

According to Guttman *et al.*[15], the situation of a chain entering the amorphous interlayer and either forming a tie chain or forming a loop is analogous to the gambler's ruin problem. According to this analysis, the probability of forming a tie chain (P_t) or forming a loop (P_l) are:

$$P_t = 1/(Z+1) \quad (5)$$

$$P_l = Z/(Z+1) \quad (6)$$

where Z is the number of statistical steps in a straight run (total length $= L_a$) between the fold surfaces. By assuming that the statistical step length is equal to the segment length projected along the chain axis (L_s), equation (7) is obtained:

$$L_a = ZL_s \quad (7)$$

Combination of equations (5), (6) and (7) leads to the following equation:

$$N_l/N_t = P_l/P_t = L_a/L_s \quad (8)$$

The concentration, N_t, of tie chains can be expressed as a combination of equations (3), (4) and (8):

$$N_t = (N_{eo}\cos\theta - L_c\rho_c/(W_cM))/(1 - L_c\rho_c(1 - W_c)/(W_c\rho_aL_s) \quad (9)$$

The molar fractions of entries of tie chains (X_t), loops (X_l) and cilia (X_c) of the fold surface are then calculated as follows:

$$X_t = N_t/(N_{eo}\cos\theta) \quad (10)$$

$$X_l = (N_{eo}\cos\theta - \rho_cL_c/(W_cM) - N_t)/(N_{eo}\cos\theta) \quad (11)$$

$$X_c = L_c\rho_c/(W_cMN_{eo}\cos\theta) \quad (12)$$

The following literature data for linear PE are inserted in equations (10)–(12); $\rho_c = 1000\,kg\,m^{-3}$ [17]; $\rho_a = 854\,kg\,m^{-3}$ [17]; $L_s = 0.125 \times 10^{-9}\,m$ [18] and $N_{eo} = 9.28 \times 10^{-9}\,kmol\,m^{-2}$ (orthorhombic unit cell: $a = 0.739\,nm$, $b = 0.493\,nm$ [18]); and the final equations are obtained:

$$X_t = \frac{1 - 1.0776 \times 10^{11}L_c/(W_cM\cos\theta)}{1 + 9.37 \times 10^{9}L_c(1 - W_c)/W_c} \quad (13)$$

$$X_l = 1 - 1.0776 \times 10^{11}L_c/(W_cM\cos\theta) - X_t \quad (14)$$

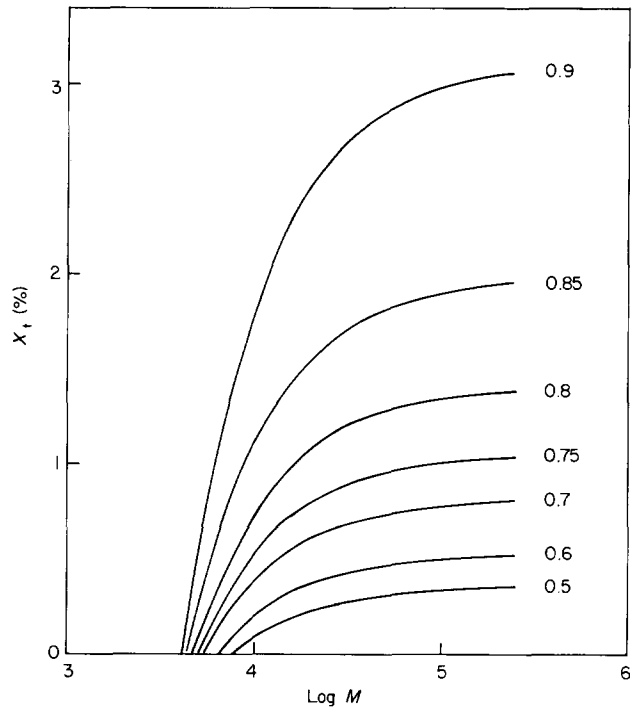

Figure 4 Molar fraction of tie chain entries in the fold surface (X_t) plotted as a function of molecular weight (M) for different crystallinity values as indicated by the figure adjacent to each curve. X_t is calculated according to equation (13) with $L_c = 30$ nm and $\theta = 30°$

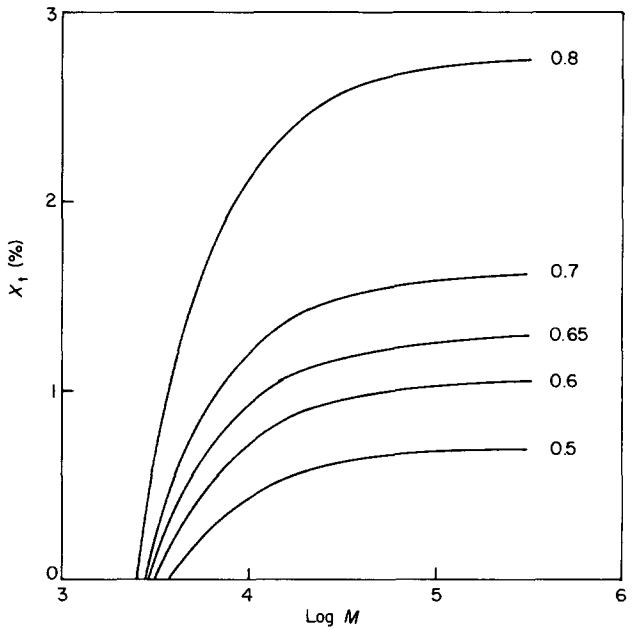

Figure 5 Molar fraction of the tie chain entries in the fold surface (X_t) plotted as a function of molecular weight (M) for different crystallinity values as indicated by the figure adjacent to each curve. X_t is calculated according to equation (13) with $L_c = 15$ nm and $\theta = 30°$

$$X_c = 1.0776 \times 10^{11}L_c/(W_cM\cos\theta) \quad (15)$$

The data obtained by the model calculation of X_t (see *Figures 4–6*) exhibit the expected molecular weight dependence with a pronounced increase of X_t with increasing molecular weight in the low molecular weight region and a less pronounced increase of X_t with increasing molecular weight at higher molecular weights.

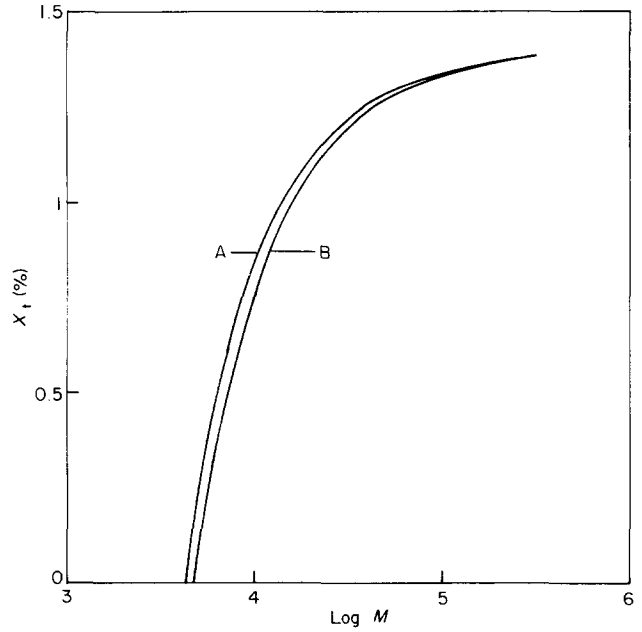

Figure 6 Molar fraction of tie chain entries in the fold surface (X_t) plotted as a function of molecular weight (M) for different chain tilt angle values. Curve A: $\theta = 0°$; curve B: $\theta = 30°$. X_t is calculated according to equation (13) with $L_c = 30$ nm and $W_c = 0.80$

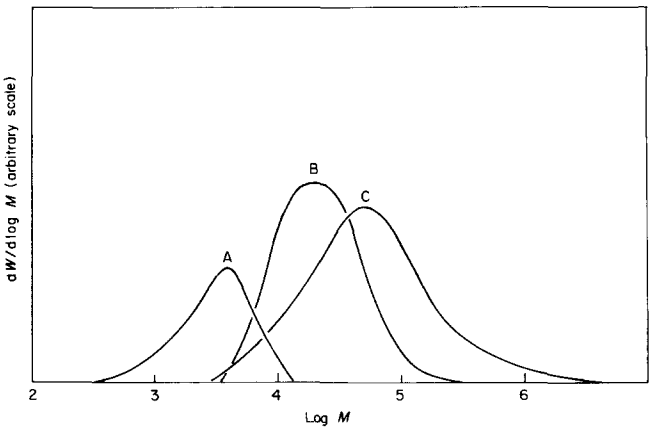

Figure 7 Molecular weight distribution for molecular weight segregated component (curve A), chain branch segregated component (curve B) and non-segregated component (curve C)

It should be noted that X_t is defined, i.e. is larger than zero, only for the following molecular weights:

$$M \geqslant L_c \rho_c / (N_{eo} \cos\theta W_c) = 1.08225 \times 10^{11} L_c / (\cos\theta W_c) \quad (16)$$

Low molecular weight material has to have a low value of the quotient $L_c/(\cos\theta W_c)$ in order to have a positive X_t and this is thus analogous with a thin amorphous interlayer.

Another interesting feature of the model which is most clearly shown in *Figures 4* and *5* is the influence on X_t of the thickness of the amorphous interlayer (L_a). At a certain molecular weight, the concentration of tie chains increases with decreasing L_a. This is demonstrated in *Figure 4*, in which X_t increases with increasing crystallinity for all combinations of L_c, θ and M.

The concentration of tie chains decreases with increasing tilt angle, particularly at low molecular weights (*Figure 6*).

When the model calculations are applied to sample 7006-IC, the following results are obtained:

This sample is considered to consist of two components: a *non-segregated* component relating to the isothermally crystallized part of the sample (high molecular weight material as shown in *Figure 7*) and a *segregated* component relating to the fraction of the sample which has not been able to crystallize isothermally at 398.2 K but has crystallized at lower temperatures during the subsequent cooling stage (low molecular weight material as shown in *Figure 7*).

Non-segregated component: The following data, presented in previously published papers[2,3], are inserted in equations (13)–(15): $\bar{M}_w = 126\,000$, $L_c = 30$–35 nm, $W_c = 0.82$, $\theta = 30°$ (estimated value based on data presented by Dlugosz *et al.*[19]).

$$X_t = 1.4\text{–}1.6\%;\ X_l = 94.1\text{–}94.7\%;\ X_c = 3.7\text{–}4.5\%$$

Segregated component: As has been shown in a previous paper[3] this component can be further divided into two parts, a purely molecular weight segregated component (*Figure 7*, curve A) and a chain branch segregated component (*Figure 7*, curve B). The following data, presented in previous reports[2,3] are inserted in equations (13)–(15):

The material represented by curve A in *Figure 7* amounts to about 30% of the segregated component, $\bar{M}_w = 3700$, $L_c = 12.3$ nm, $W_c = 0.65$, $\theta = 30°$ (estimated value based on data by Dlugosz *et al.*[19]).

$$X_t = 0.6\%;\ X_l = 37.3\%;\ X_c = 62.1\%$$

The material represented by curve B in *Figure 7* amounts to about 70% of the segregated component, $\bar{M}_w = 29\,000$, $L_c = 12.3$ nm, $W_c = 0.65$, $\theta = 30°$ (estimated value based on data by Dlugosz *et al.*[19]).

$$X_t = 1.4\%;\ X_l = 90.5\%;\ X_c = 8.1\%$$

Total segregated component: $\bar{M}_w = 17\,000$, $L_c = 12.3$ nm, $W_c = 0.65$, $\theta = 30°$ (estimated value based on data by Dlugosz *et al.*[19]).

$$X_t = 1.3\%;\ X_l = 84.5\%;\ X_c = 14.2\%$$

These calculations show that the 'curve A material' has the lowest X_t value, about one-third of that of the non-segregated component. In addition to this manifestation of weakness, the fold surface of the 'curve A fraction' is dominated by cilia, i.e. 2/3 of the entries of the fold surface in this part of the sample are cilia. According to this analysis, both the curve B fraction and the total segregated component are only marginally weaker than the non-segregated component.

The 'input' data for the components considered are all average data. Each component shows a distribution in all of the 'input' variables (see *Figure 7*). It is obvious that the low molecular weight tail of the curve A material, if it exists in isolation, constitutes the weakest part of the material.

An important factor for the results of the model calculation is the number of statistical steps in a straight run between the fold surfaces. The simple assumption made earlier, that the statistical step is analogous to the carbon–carbon segment should only be considered as a rough, first approximation. It is known that different factors such as bond angle, preferred conformational state and volume exclusion effects make the chain less flexible and the statistical length greater by a factor of α than the primary segment length. Such a consideration influences the molar fractions of tie chains, loops and cilia (equations (10)–(12)) in the following way:

$$X_t = X_{t,\alpha=1}\alpha \tag{17}$$

$$X_l = 1 - X_{t,\alpha=1}\alpha - X_{c,\alpha=1} \tag{18}$$

$$X_c = X_{c,\alpha=1} \tag{19}$$

Thus, X_t increases with increasing α at the expense of X_l. However, the *relative* differences in X_t obtained for the segregated and the non-segregated component remain unchanged.

The regions containing the segregated molecules can therefore be expected to be significantly weaker than other parts of the structure and thus to act as fracture initiators and fracture transmitters. Fracture should propagate more easily through these regions than elsewhere. There are experimental data showing that segregated low molecular weight material is essentially concentrated in the spherulite boundaries and/or localized between main lamellae within the spherulites[9].

Fracture thus propagates preferably through regions of segregated low molecular weight material located at the spherulite boundaries (modes I and II) or within the spherulites between main lamellae (mode III). Systems with large spherulites, formed as a consequence of high temperature and/or low nucleation density, with a high concentration of segregated low molecular weight material, frequently fracture according to mode III (*Figure 1c*). Systems with smaller spherulites with a lower concentration of segregated low molecular weight material fracture more frequently according to modes I and II (*Figures 1a, b*). These findings are consistent with observations by Keith and Padden[7]. Systems with large and coarse spherulites fracture almost independently of spherulite structure, whereas systems with smaller spherulites fracture in the spherulite boundaries.

As shown in a previous paper[2], molecular weight segregation also occurs to some extent in systems rapidly cooled from the melt. The low molecular weight material accumulates at the spherulite boundaries and between main lamellae within the spherulites precisely as for systems isothermally crystallized from the melt[9]. This is most probably the main reason for the similarity in the appearance of the fracture surfaces of the IC and RC samples (compare *Figures 1a* and *c*).

The development of fracture in high molecular weight PE

In the high molecular weight systems, 2912 and 2215 in this study, the fracture behaviour is more complicated and depends strongly on the applied stress:

(a) At the highest levels, fracture is brittle[21].
(b) At somewhat lower stresses, fracture is ductile[10,21]. A fibrous material is formed which fractures at some later stage[10,21].
(c) At even lower stress levels, fracture is again macroscopically brittle[10,21]. From a practical point of view this type of fracture is extremely interesting and is the subject of this section.

As can be seen in all the micrographs in *Figure 8*, the fracture surfaces in high molecular weight material are covered with more or less developed fibrils. The fibrils become gradually more developed as the distance from the initiation region increases (*Figure 8a*). At some distance from the point of initiation, the fracture becomes macroscopically fibrous (*Figure 8a*).

In the initiation region, the fibrils are comparatively thin (smaller than 0.5 μm) and short (shorter than 10 μm) (*Figures 8b* and *c*). There seems to be no obvious connection between the fracture path and the supermolecular structure as there is in the case of low molecular weight systems. Apart from being due to the occurrence of a brittle propagation, the disruption of the plastic deformation can be due to the geometry of the micro-necking. In the rapid crack-growth region there are however some indications of heterogeneity in strength of the systems (*Figures 8d* and *e*).

Influence of thermal history on the development of fracture

Fracture data for two of the low molecular weight materials, including both IC and RC samples, are shown in *Figure 9*.

The data presented in *Figure 9* were treated in the following way:

The differences in fracture time for each pair of data (RC and IC subjected to the same stress (σ) at the same temperature (T)) were determined according to equation (20):

$$x = \log(t_f)_{RC}(\sigma,T) - \log(t_f)_{IC}(\sigma,T) \tag{20}$$

where $(t_f)_{RC}$ is the fracture time for the RC sample and $(t_f)_{IC}$ is the fracture time of the IC sample. In those cases where a small difference in stress existed, the data points were shifted to the correct stress according to the regression line.

Average values ($\bar{x}$) and standard deviations of sample (s) were determined for the two materials: $\bar{x}_{7006} = 0.37$, $s_{7006} = 0.50$; $\bar{x}_{7018} = 0.47$, $s_{7018} = 0.53$.

The hypothesis that $\bar{x} > 0$ was tested assuming a t-distribution of the average data. The variable t was determined according to equation (21):

$$t = (\bar{x} - 0)/(s/(n-1)^{1/2}) \tag{21}$$

where n is the number of data in each average. The following results were obtained for the materials studied: $t_{7006} = 2.56$ ($n = 13$), $t_{7018} = 3.07$ ($n = 13$). The probability that $\bar{x} > 0$ is according to standard tables for the t-distribution[23] 99% for material 7006 and 99.5% for 7018.

The demonstrated difference in strength of the samples can be explained on the following basis:

- Evidence that co-crystallization between components of different molecular weights occurs to a greater extent in the rapidly cooled systems (RC) than in systems crystallized at a low degree of supercooling such as e.g. the IC systems has been presented in an

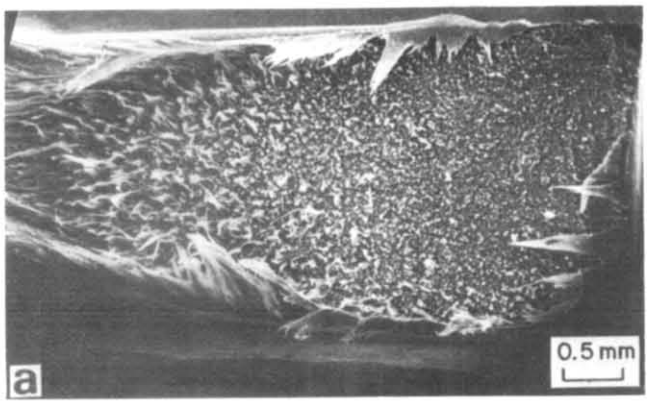

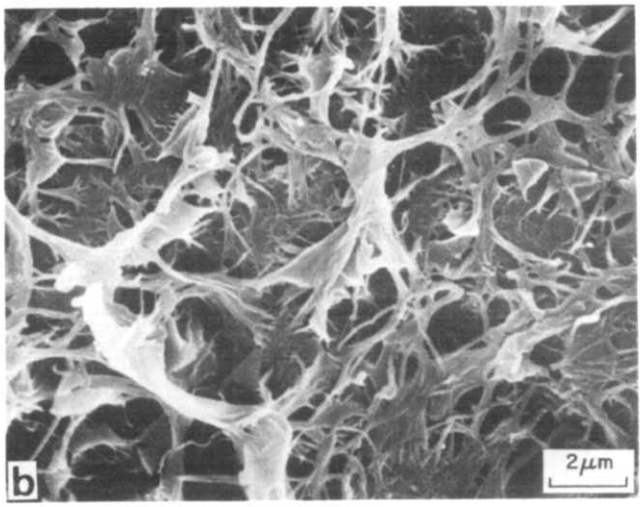

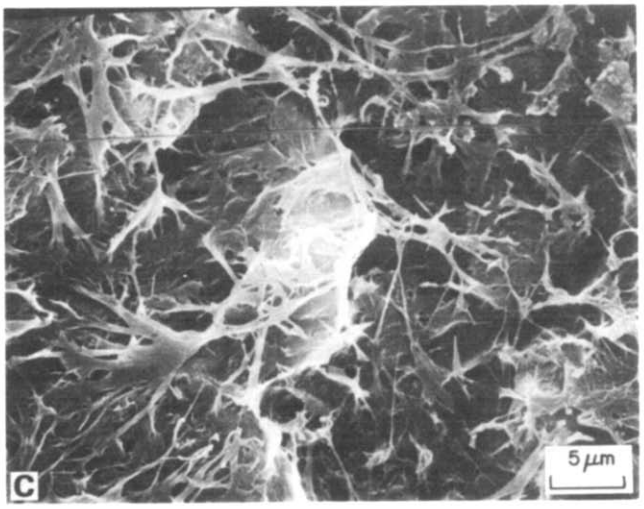

Figure 8 Scanning electron micrographs of different fracture surfaces. All the samples were fractured in water. (a) 2912-IC, stress = 5.5 MPa, $T = 343.2$ K. (b) 2912-IC, stress = 4.2 MPa, $T = 353.2$ K, in the initiation region. (c) 2912-RC, stress = 3.9 MPa, $T = 353.2$ K, in the initiation region. (d) 2912-RC, stress = 5.4 MPa, $T = 353.2$ K, some distance from the initiation region. (e) 2912-IC, stress = 4.2 MPa, $T = 353.2$ K, some distance from the initiation region

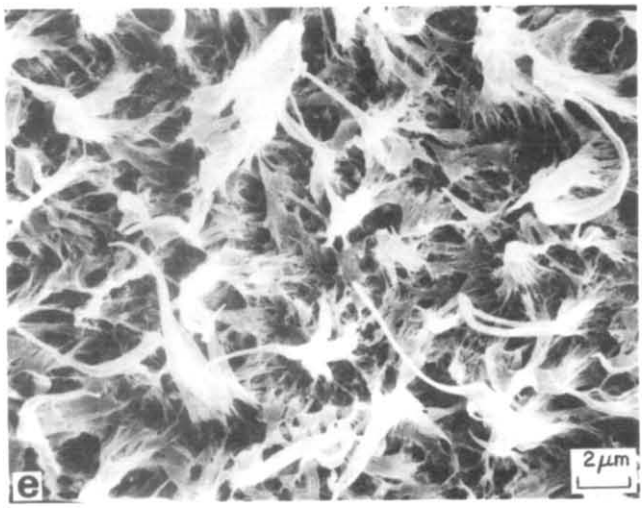

earlier paper[2]. Hence, the rejected low molecular weight material is contaminated with some high molecular weight species in the RC samples and thereby reinforced due to an increase in the number of interlamellar tie chains.

- There is reason to suppose[9] that the low molecular weight material is more evenly distributed over the structure and hence less accumulated in certain topologically continuous regions in the RC systems than in the IC systems.
- There are indications that the tie chain concentration, on an average, is higher in the rapidly cooled RC systems than in the IC systems[22].

The above data are in agreement with earlier reports by Phillips and Patel[20] and by Gedde *et al.*[1].

For the high molecular weight systems no statistically significant difference between the IC and RC systems could be observed.

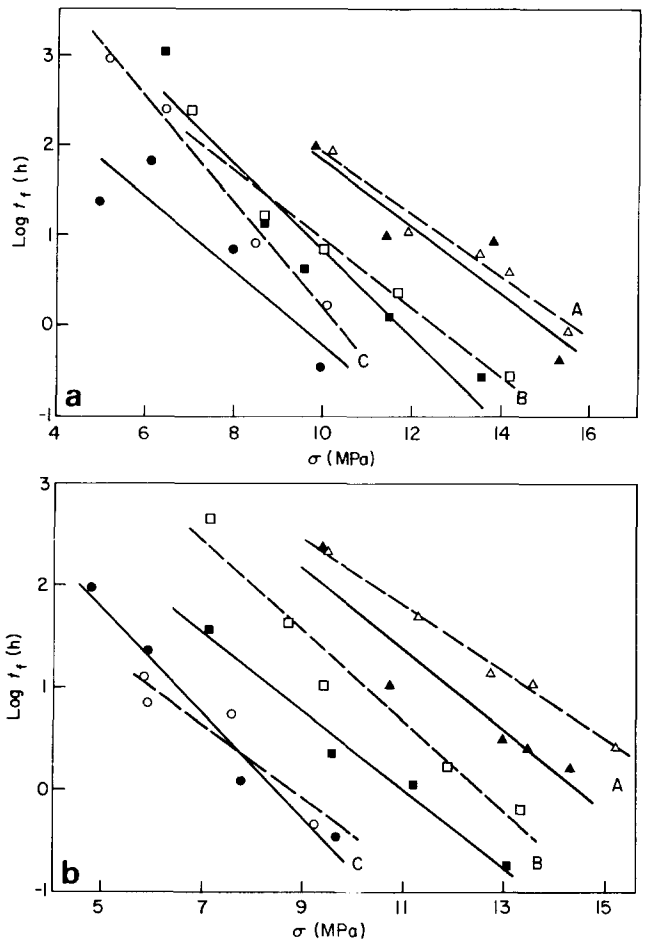

Figure 9 Fracture data (the logarithm of the time to fracture plotted vs. the nominal stress) for samples subjected to constant uniaxial tensile loads in air at different temperatures. (A), $T = 303.2$ K: (▲), IC; (△), RC. (B), $T = 318.2$ K: (■), IC: (□), RC. (C), $T = 333.2$ K: (●), IC; (○), RC. The solid regression lines are associated with the IC samples and the broken lines with the RC samples. (a) Sample 7006; (b) sample 7018

CONCLUSIONS

In the low molecular weight systems, fracture occurs according to three different modes: (i) interspherulitic propagation with reorientation; (ii) interspherulitic propagation without reorientation; (iii) trans-spherulitic interlamellar propagation. These events are controlled by the strength distribution in the structure, which originates from the occurrence of a molecular weight segregation. The latter produces a variation in molecular weight in the systems. According to a model calculation shown in this paper, the tie chain concentration is almost half an order of magnitude lower in the low molecular weight regions than elsewhere. The regions of low molecular weight are located in the spherulite boundaries and between main lamellae within the spherulites. Hence, all three fracture propagation modes can be associated with this segregated low molecular weight material.

The low molecular weight systems which had been rapidly cooled from the melt (RC) showed a higher strength than the systems isothermally crystallized at 398.2 K (IC). This difference can be assigned to the following causes: (i) a reinforcement of the weakest regions of the structure caused by an increased tendency for co-crystallization between components of different molecular weight in the RC systems; (ii) a more advantageous distribution in the structure of the weak low molecular weight species in the RC systems; and (iii) a higher concentration, on an average, of interlamellar tie chains in the RC systems.

The fracture surfaces of the high molecular weight systems revealed less information concerning variations in the strength of the structure. The formation of bundles of more or less connected fibrils can be due both to local brittleness and to the geometry of the micro-necking.

ACKNOWLEDGEMENTS

The reported studies are parts of a research programme on crystalline polymers sponsored by the National Swedish Board for Technical Development (STU) and by the Swedish Natural Science Research Council (NFR). The authors wish to thank Mr S. Eklund in this department for experimental assistance, Dr C. Blomberg at the Department of Theoretical Physics, The Royal Institute of Technology, Stockholm for valuable discussions and Unifos Kemi AB, Sweden, for supplying the polyethylenes studied.

REFERENCES

1 Gedde, U. W., Terselius, B. and Jansson, J.-F. *Polym. Eng. Sci.* 1981, **21**, 172
2 Gedde, U. W. and Jansson, J.-F. *Polymer* 1983, **24**, 1521
3 Gedde, U. W., Eklund, S. and Jansson, J.-F. *Polymer* 1983, **24**, 1532
4 Gedde, U. W., Eklund, S. and Jansson, J.-F. *Polymer Bull.* 1982, **9**, 90
5 Anderson, F. R. *J. Appl. Phys.* 1964, **35**, 64
6 Yu, Y.-F. and Ullman, R. *J. Polym. Sci.* 1962, **60**, 55
7 Keith, H. D. and Padden Jr., F. J. *J. Polym. Sci.* 1959, **41**, 525
8 Fotheringham, D. and Parker, B. *J. Mater. Sci., Lett.* 1976, **11**, 979
9 Gedde, U. W. and Jansson, J.-F. *Polymer* 1984, **25**, 1263
10 Gedde, U. W. and Jansson, J.-F. *Polym. Eng. Sci.* 1980, **20**, 579
11 Kausch, H. H. in 'Polymer Fracture', 1978, Springer Verlag, Berlin
12 Becht, J. and Fischer, K. *Koll. Z. Z. Polym.* 1969, **229**, 167
13 Kausch, H. H. and Becht, J. *Rheol. Acta* 1970, **9**, 137
14 Stein, R. S. *Acc. Chem. Res.* 1972, **5**, 121
15 Keller, A. and Priest, D. J. *J. Macromol. Sci.* 1968, **B2**, 479
16 Guttman, C. M., DiMarzio, E. A. and Hoffman, J. D. *Polymer* 1981, **22**, 1466
17 Wunderlich, B. 'Macromolecular Physics', Vol. 1, 1973, Academic Press, New York
18 Kavesh, S. and Schultz, J. M. *J. Polym. Sci., Polym. Phys. Edn.* 1970, **8**, 243
19 Dlugosz, J., Fraser, G. V., Grubb, D., Keller, A., Odell, J. A. and Goggin, P. L. *Polymer* 1976, **17**, 471
20 Phillips, P. J. and Patel, J. *Polym. Eng. Sci.* 1978, **18**, 943
21 Zapas, L. J. and Crissman, J. M. *Polym. Eng. Sci.* 1979, **19**, 104
22 Sadler, D. M. and Keller, A. *Macromolecules* 1977, **10**, 1128
23 Spiegel, M. R. 'Probability and Statistics', McGraw-Hill Book Company, New York, 1975